# Time-dependent density-functional-theory investigation of the collisions of protons and α particles with uracil and adenine

Cody Covington, Kara Hartig, Arthur Russakoff, Ryan Kulpins, and Kálmán Varga*
*Department of Physics and Astronomy, Vanderbilt University, Nashville, Tennessee 37235, USA*
(Received 6 February 2017; published 9 May 2017)

Time-dependent density-functional theory was employed to study the effects of proton and α-particle radiation on uracil and adenine. This method has the advantage of treating nuclear motion and electronic motion simultaneously, allowing for the study of electronic excitation, charge transfer, ionization, and nuclear motion. Particle energies were surveyed in the range of 15–500 keV for protons and 100–2000 keV for α particles in conjunction with impact points both on and off carbon bonds in order to investigate the electron and nuclear dynamics of irradiated molecules and the form and quantity of transferred energy. The stopping power, energy transferred, and ionization were found, and the relationship between incident particle energy and electron density of the target molecule was characterized for proton and α-particle radiation incident on adenine and uracil.

DOI: 10.1103/PhysRevA.95.052701

## I. INTRODUCTION

Understanding how biological molecules react to radiation on the nanoscale is a challenge that transcends physics, chemistry, and biology and that has only relatively recently been addressable via advances in instrumentation and computational capabilities [1–22]. While many of the biological consequences of radiation have been observed and tested on the macroscale, including cancer, birth defects, heart disease, and central nervous system diseases [4,23,24], the experimental limitations have, until recently, prevented direct observation of its mechanisms and immediate effects on the molecular scale. This topic is currently of particular interest to the advancement of ion radiation therapy, which has emerged as an outstanding candidate for cancer treatment since it allows for precise dose localization [25–28]. This is because radiation damage caused by charged particles follows the Bragg curve [28–30], which is caused by a resonance between the ion's speed and the electrons in the medium. This resonance results in minimal energy deposition at high particle energies that increases sharply to a peak just before the particle stops [31,32].

Experiments to probe the ionization and fragmentation of atoms and molecules face great challenges, as the primary and secondary damage from radiation occurs on the attosecond to nanosecond time scale. Also, due to the size and difficulty of isolation, measurements are currently limited with respect to biological molecules in their native (aqueous) environment. Currently, most of our understanding comes from studies in the gas phase, where the effects of proton and other ion collisions on small molecules have been investigated [5,8,33–41]. The resulting fragments can then be used to determine the most common fragmentation channels for a given particle energy.

Since the 1950s, scientists have studied the interactions of atoms and molecules with fast moving particles using theoretical models [42–44]. These methods range from the first and second Born approximations [45,46] to more advanced fully quantum and nonperturbative treatments [47–62].

Computational methods have also been developed to aid in the study of radiation's effects on biological systems. These studies seek to explore key mechanisms of radiation damage: the role of velocity and charge of the radiated particle and the medium through which it travels. A popular and powerful computational approach to achieve this goal is Monte Carlo track-structure simulations, which provide a detailed event-by-event description of the primary and secondary damage caused by ionizing radiation [9–11,30,63–65]. The track-structure simulations require knowledge of the interaction cross section (or ionization and excitation cross sections) for the medium, which can be explicitly calculated, approximated from the dielectric function, or taken from experimental data [31,32,63,66–68]. An important consideration for secondary damage, however, is that the interaction cross section is affected by various ionization mechanisms [8,50,69–74]. Therefore, correctly modeling the overall damage by radiation requires proper treatment of ionization.

To better understand radiation effects, one has to characterize the ion energies at which these constituents reach excited electronic states, ionize, fragment, or otherwise degrade upon exposure to radiation. In this paper, we will use the time-dependent density-functional theory (TDDFT) [75] to study electronic and nuclear dynamics in particle irradiation of uracil and adenine. TDDFT has proven to be a very powerful computational tool to simulate electronic excitation and ionization in molecular systems [76–81]. We have developed several different computational approaches [82–84] to make TDDFT calculations more efficient and accurate, and in a recent work we described the collision of energetic ions and graphene fragments in this framework [85].

First-principles theoretical calculations have recently become popular tools in studying radiation's effects on molecules of biological importance in such studies. These works include the description of the fragmentation of protonated [22] and doubly charged uracil [21], which well reproduces fragmentation channels observed in experiment. Additional studies have been performed on ion collisions with gas-phase and aqueous uracil [18,20], although these studies were limited by treating ionization as an instantaneous loss of electrons. Other studies have modeled collisions with heavier ions [16,17]. Simulations have also been performed that include the electron dynamics in the collision using various theoretical treatments, but these calculations used atomic-orbital (Gaussian based) basis sets

*kalman.varga@vanderbilt.edu

 

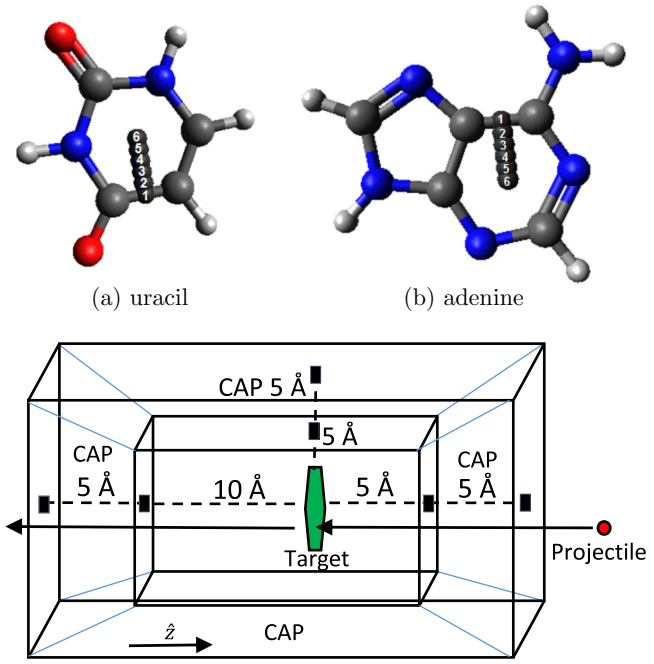


(a) uracil (b) adenine

(c) simulation geometry

FIG. 1. (a) Uracil and (b) adenine; carbon is gray, nitrogen is blue, oxygen is red, and hydrogen is white. The black points represent the six impact points. (c) The simulation geometry is also shown.

on various small molecules [12–15]. However, localization of the wave function from a limited Gaussian basis will prevent electrons from ionizing into continuum states, and studies of such radiation-molecular interactions using real-space grids could better model the ionization process [78,80,81,85,86].

In this work we will use TDDFT and Ehrenfest molecular dynamics with a real-space representation to study the ionization of two molecules of biological importance, namely, uracil and adenine, subject to impacts from protons and $\alpha$ particles. Ion collisions with uracil and adenine will be studied as a function of impact point and particle energy, ranging from 15 to 500 keV for protons and 100 to 2000 keV for $\alpha$ particles. The structures of uracil, a constituent of RNA, and adenine, a constituent of RNA and DNA, are shown in Fig. 1. To sample the dependence of the geometry of the molecule with respect to the projectile, we use two strategies for choosing the impact points. In the first case, the dependence on a given bond is investigated by gradually moving the impact point (see Fig. 1) in order to sample various electron densities in proximity to carbon-carbon bonds. In the second case, a large set of random geometries (impact points and angles) is generated.

## II. COMPUTATIONAL METHOD

The computations were performed using density-functional theory (DFT), with the Kohn-Sham (KS) Hamiltonian of the form [75]

$$H_{\rm KS}(t) = T + V_{\rm H}[\rho](\mathbf{r},t) + V_{\rm XC}[\rho](\mathbf{r},t) + V_{\rm ion}(\mathbf{r},t) + V_{\rm P}(\mathbf{r},t). \quad (1)$$

Here $T$ is the kinetic-energy operator, and $\rho$ is the electron density, which is defined by a sum over all occupied orbitals:

$$\rho(\mathbf{r},t) = \sum_{k=1}^{N_{\rm orbitals}} 2|\psi_k(\mathbf{r},t)|^2, \quad (2)$$

where the coefficient 2 accounts for the number of electrons in each orbital. $V_{\rm H}$ is the Hartree potential, defined as

$$V_{\rm H}(\mathbf{r},t) = \int d\mathbf{r}' \frac{\rho(\mathbf{r}',t)}{|\mathbf{r}-\mathbf{r}'|}, \quad (3)$$

which accounts for the mean electrostatic interactions from electron-electron repulsion. $V_{\rm XC}$ is the exchange-correlation potential, which is approximated by the local-density approximation, obtained from a parametrization to a homogeneous electron gas by Perdew and Zunger [87]. $V_{\rm ion}$ is the external potential due to the ions, represented by employing norm-conserving pseudopotentials centered at each ion as given by Troullier and Martins [88]. The $V_{\rm P}$ term accounts for the Coulomb potential of the projectile.

The time evolution of the electronic wave function was achieved using the time-dependent KS equation, given as

$$i\hbar\frac{\partial\psi_k(\mathbf{r},t)}{\partial t} = H_{KS}\psi_k(\mathbf{r},t). \quad (4)$$

Equation (4) was solved using the following time propagator:

$$\psi_k(\mathbf{r},t+\delta t) = \exp\left[\frac{-i}{\hbar}H_{KS}(t)\delta t\right]\psi_k(\mathbf{r},t). \quad (5)$$

This operator was approximated using a fourth-degree Taylor expansion, given as

$$\psi_k(\mathbf{r},t+\delta t) \approx \sum_{n=0}^{4}\frac{1}{n!}\left(\frac{-i\delta t}{\hbar}H_{KS}(t)\right)^n\psi_k(\mathbf{r},t). \quad (6)$$

A time step of $\delta t = 1$ as was used in the simulations.

The nuclear motion was treated, using Ehrenfest dynamics [89] via Newton's second law, as

$$M_i\frac{d^2\mathbf{R_i}}{dt^2} = \sum_{i\neq j}^{N_{\rm ions}}\frac{Z_iZ_j(\mathbf{R_i}-\mathbf{R_j})}{|\mathbf{R_i}-\mathbf{R_j}|^3} - \nabla_{\mathbf{R_i}}\int V_{\rm ion}(\mathbf{r},\mathbf{R_i})\rho(\mathbf{r},t)d\mathbf{r}, \quad (7)$$

where $M_i$, $Z_i$, and $\mathbf{R_i}$ are the mass, charge, and position of the $i$th ion, respectively. This differential equation was time propagated using the Verlet algorithm at every time step.

Since the projectile moves at much higher speeds than the nuclei that constitute the molecular system, the forces experienced by the projectile were represented as being strictly Coulombic, given as

$$M_p\frac{d^2\mathbf{R_p}}{dt^2} = \sum_{i}^{N_{\rm ions}}\frac{Z_iZ_p(\mathbf{R_i}-\mathbf{R_p})}{|\mathbf{R_i}-\mathbf{R_p}|^3} - Z_p\int\rho(\mathbf{r},t)\frac{(\mathbf{r}-\mathbf{R_p}+\beta)}{|\mathbf{r}-\mathbf{R_p}+\beta|^3}d\mathbf{r}, \quad (8)$$

where $\mathbf{R_p}$ is the position of the projectile and $\beta$ is the soft Coulomb (SC) parameter described below. The projectile equations of motion were time propagated every time step.

The wave function of valence electrons was represented using a real-space grid. To prevent reflections from the boundary of the simulation box, a complex absorbing potential (CAP) of the form developed by Manolopoulos [90] was used. A grid spacing of 0.25 Å was chosen for all simulations described. The total simulation box extended 10 Å beyond the edges of the molecule in the $xy$ plane, allowing 5 Å for bound electron dynamics and another 5 Å for the CAP. Along the $z$ axis, the target molecule was given additional room for 10 Å of electron dynamics (refer to Fig. 1 for simulation box geometry). The projectiles were given an initial velocity, determined by their kinetic energy, only in the $-\hat{z}$ direction. The starting position of the projectiles was 17.5 Å away from the molecule along the $z$ axis with the $x$ and $y$ coordinates matching an impact point.

Because a real-space grid was used, the Coulombic potential of the projectile, the $V_{\mathrm{P}}$ term in the Hamiltonian, was represented with a SC potential, given as [91]

$$V(\beta, Q; x) = -\frac{Q^2}{(\beta^2 + x^2)^{1/2}}. \tag{9}$$

In the literature, $\beta$ is usually set to a value in the range of 1–2 bohrs [91–94]. The value of $\beta$ changes the energy levels and ionization potential and ideally should be as small as the grid spacing will allow. To compare the effect of the SC potential parameter $\beta$ on the system, ground-state calculations were performed using the atomic orbital basis formed from Gaussian basis functions, specifically the 6-311G** basis set. A proton or an $\alpha$ particle was added to uracil at several positions on and off of grid points; then the energy was compared between the Gaussian basis and the grid. Comparison of these energies revealed poor correlation for values of $\beta$ below 0.2, and therefore, $\beta$ was set as 0.2 for all calculations. The Gaussian basis calculations were performed using the software package NWCHEM [95].

The effect of the projectile on the molecule was characterized by the local electron density encountered by the projectile along its path of travel. Since the projectile may have a scattering cross section that depends upon the incident velocity, a one-dimensional line integral was chosen to represent the total electron density encountered by the incident particle, given as

$$\rho_\gamma = \int_C \rho(\mathbf{r}) d\mathbf{s}, \tag{10}$$

where the contour follows the ideal path of the projectile. The ground-state electron density was used to calculate $\rho_\gamma$. The Akima interpolation method was used to interpolate the values of $\rho(\mathbf{r})$ between the real-space grid points of the simulation [96,97].

Two sets of impact points were used. The first set was selected to systematically sample a given bond (see Fig. 1), and the second set was chosen randomly. In the second case a set of 200 random impact points at random incidence angles were made by rotating and displacing uracil randomly, with the criteria that the projectile must pass within 3 Å of an atom in the molecule. This distance was selected because simulations showed that at distances greater than 3 Å from a nucleus the ionization is less than 2% and the energy transfer is less than 0.5 eV at resonant proton speeds. Only three near-resonant proton energies were used for the random impact points due to the computational burden of such a large number of simulations.

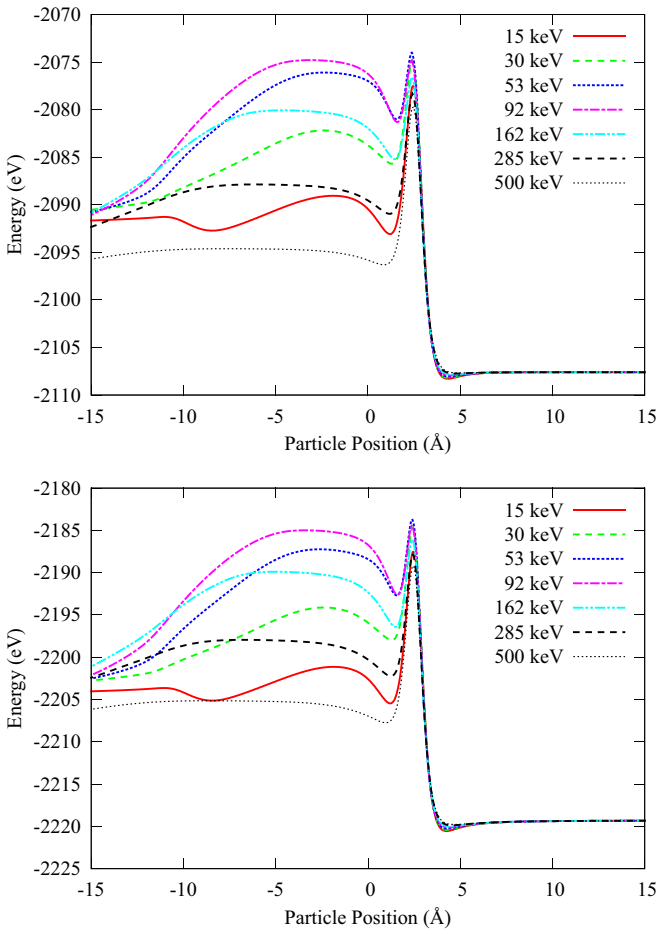


FIG. 2. Proton simulations: Energy as a function of particle trajectory for uracil (top) and adenine (bottom) at various proton energies incident upon impact point 1. The molecule is located at 2.5 Å; the proton approaches from the right.

## III. RESULTS

### A. Energy transfer

The energy transferred to the molecule can be determined by analyzing the system energy as a function of projectile position, shown in Fig. 2 for impact point 1. The simulations exhibit a strong peak in energy just as the particle reaches the molecule due to the Coulombic repulsion with the nuclei. After passing through the molecule, the rapidly changing potential imparts energy to the electrons causing ionization. Finally, the system relaxes into its new electronic configuration.

The process of projectile impact can be further understood by considering the time-dependent electron density, a few snapshots of which are shown in Fig. 3. As the projectile enters, electron density is accelerated towards the projectile. As the projectile passes through the molecule, it encounters areas of higher electron density. The potential from the projectile causes an energy shift of the orbitals, and due to the rapid, nonadiabatic change, they are now in an excited state. The rapid transit of the projectile (0.85- to 1.075-fs frames in

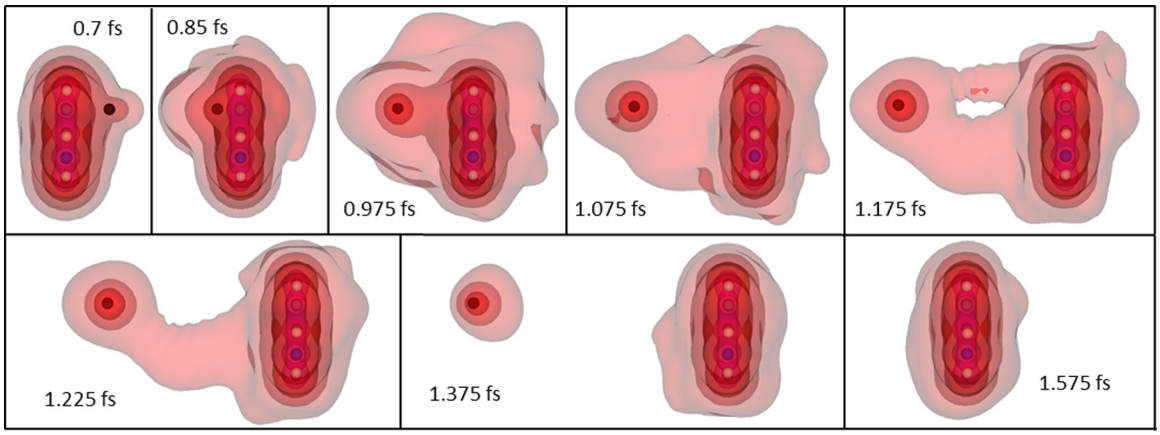


FIG. 3. Snapshots of electron density isosurfaces of a uracil 100 keV $\alpha$-particle collision at carbon-carbon bond impact point 1. Various times throughout the ionization process are shown with isodensity values of 1, 0.1, 0.01, and 0.001.

Fig. 3) removes the potential and imparts kinetic energy, which causes ionization. Also, some orbitals have acquired enough kinetic energy to localize onto the moving potential, meaning the projectile has captured some electron density. As the simulation proceeds (1.225- to 1.575-fs frames in Fig. 3), electron density relaxes back onto the molecule or localizes onto the projectile. As seen in the snapshots after the projectile has passed through the molecule, the electronic wave function is spread out over a large area, indicating that the use of a localized basis (such as a limited Gaussian basis) would not allow for the freedom to delocalize and ionize to continuum states.

Simulations with $\alpha$ particles have the same features as the proton simulations, shown in Fig. 4; however, after impact they exhibit oscillations in energy at lower projectile energies due to oscillations of the electron density localized on the projectile and due to regions of delocalized electron density recolliding with the molecule (see Fig. 3).

The energy transferred to the molecule can be determined for proton radiation by picking the maximum energy after the projectile has exited the molecule and subtracting out the initial energy. The kinetic energy of the nuclei for these impact points is negligible ($< 0.1$eV) at such short times following the collision. Therefore, this energy difference would be the total energy obtained by all electrons due to the collision, including ones that are subsequently ionized. The results of the energy transfer are to ultimately cause ionization, electronic excitation, or nuclear motion. Since the $\alpha$-particle simulations had some oscillations in the total energy in this region, the energy transferred to the molecule was taken to be the average of the energy while the projectile was between 0 and $-7.5$ Å.

The energy transferred as a function of projectile energy is a particularly useful quantity, as it governs molecular fragmentation and indicates the sensitivity of a biomolecule to radiation. The amount of energy transferred is also dependent upon the region that the projectile passes through. When simulations of the same energy are compared for various carbon-carbon bond impact points, very similar curves can be seen, as shown in Fig. 5. For the $\alpha$-particle simulations, even the oscillations in energy are present in the same places (approximately 0 and $-7$ Å).

In order reduce the number of data points and fit variables, only one projectile energy was compared to electron density. This energy was chosen to correspond to the strongest projectile-molecule interaction (maximum energy transfer)

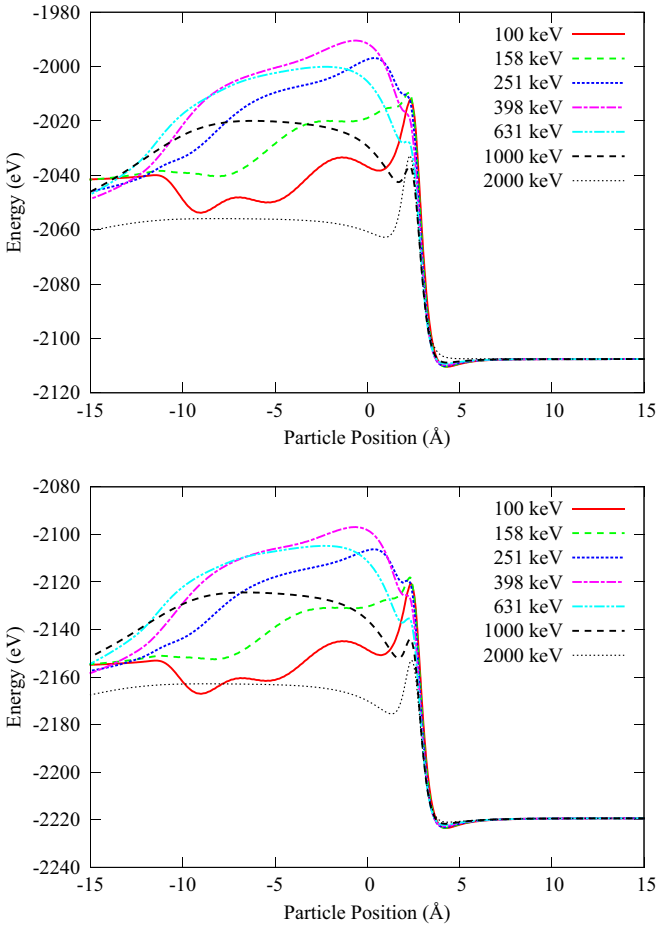


FIG. 4. The $\alpha$-particle simulations: Energy as a function of particle trajectory for uracil (top) and adenine (bottom) at various $\alpha$-particle energies, incident upon carbon-carbon bond impact point 1. The molecule is located at 2.5 Å; the projectile approaches from the right.

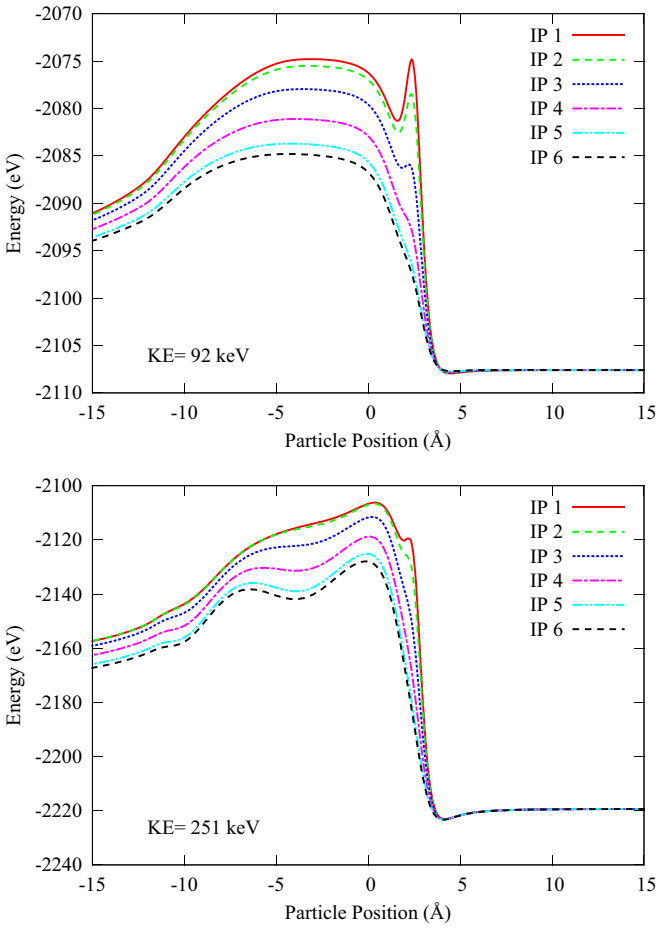


FIG. 5. System energy as a function of particle trajectory for various carbon-carbon bond impact points (IPs) showing uracil-proton (top) and adenine–$\alpha$-particle (bottom) simulations. The molecule is located at 2.5 Å; the projectile approaches from the right.

and was used for analysis of trends in the energy transfer with respect to electron density. The projectile energy (speed) with the maximum energy transfer for a given impact point was found by fitting a plot of the energy transferred to the molecule vs projectile energy (in logarithmic scale) to a sixth-degree polynomial, as shown in Fig. 6.

The maximum energy transferred to the molecule can be correlated to the electron density that the projectile encounters $\rho_\gamma$, as shown in Fig. 7 for protons and $\alpha$ particles. A simple relationship can be seen between the two, which indicates that the scattering process at resonant energies may be approximated using only the ground-state electron density. The relationship is approximately logarithmic, indicating that the maximum energy transfer can be significant even when the projectile does not pass directly through any chemical bonds. The results of the fits to the data are reported in Table I.

The simulations indicate that the projectile will lose more energy as it passes through regions of higher electron density, as one would expect. However, the key finding is the simple relationship between electron density and peak energy transfer, which is a promising result for further simulations of DNA damage from particle radiation. The energy curves reveal that adenine absorbs slightly more energy than uracil, which may

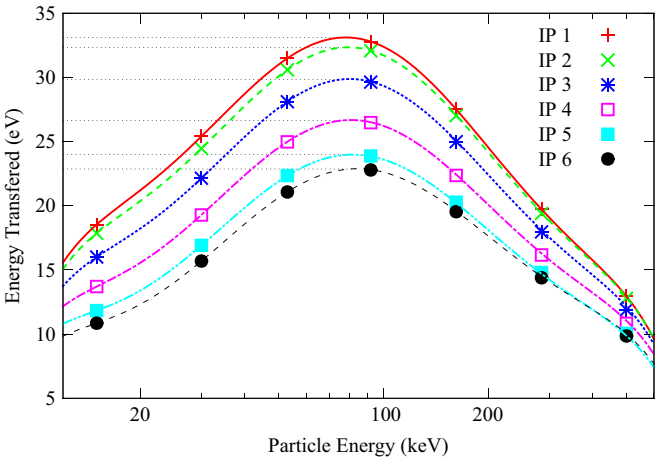


FIG. 6. Energies imparted to uracil as a function of proton energy fitted to a sixth-degree polynomial for various carbon-carbon bond impact points (IPs). Finely dashed lines show the local maxima for each curve.

be caused by the larger number of electrons in adenine or by its lower energy of −2219 eV compared to −2108 eV for uracil. The logarithmic fits to the electron density are of poorer quality for the $\alpha$-particle simulations than the proton simulations, as evidenced by larger relative errors in the fit parameters. This could be due to the oscillations in the energy after the $\alpha$ particle exits from the molecule, introducing error into the maximum energy.

### B. Stopping power

An analysis similar to that given above can also be performed with projectile energy in the place of molecule energy to describe the stopping power of uracil and adenine and the effects of impact on the projectile. The stopping power is a measure of how much energy a particle loses per unit length traveled. The change in projectile energy was found by taking the difference between the projectile's initial and final kinetic energies, in this case at −15 Å, which corresponds to the complete ionization of the projectile in the CAP. Since the particle loses energy during interaction with the molecule, the change in energy is negative. The particle speed that lost the most energy in the collision was determined by the same fitting procedure used for the energy transfer in Sec. III A. The maximum projectile energy lost was plotted versus the electron density for each carbon-carbon bond impact point

TABLE I. Parameters from the least-squares fit of $y=a\log_{10}x+b$ to the maximum energy transferred and electron density data for carbon-carbon bond impact points.

| Molecule | Particle | $a$ | $b$ |
|---|---|---|---|
| Uracil | Proton | 11.55 ± 0.16 | 29.55 ± 0.06 |
| Adenine | Proton | 12.02 ± 0.19 | 30.47 ± 0.06 |
| Uracil | $\alpha$ particle | 27.3 ± 0.6 | 102.98 ± 0.21 |
| Adenine | $\alpha$ particle | 30 ± 1 | 107.73 ± 0.33 |

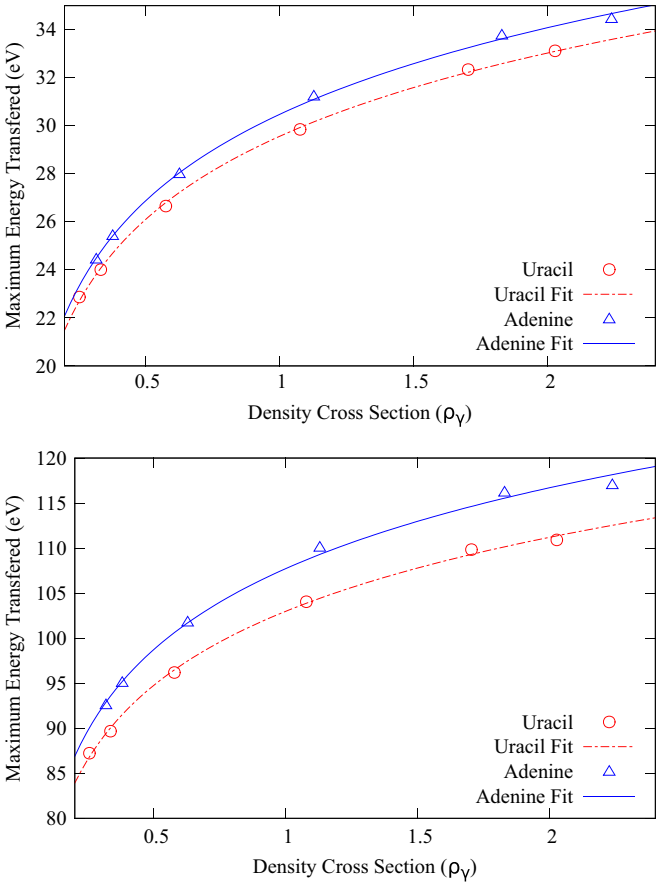


FIG. 7. Maximum energy imparted to the molecule as a function of electron density for proton (top) and $\alpha$-particle (bottom) simulations for carbon-carbon bond impact points. A fit to a logarithmic function is shown.

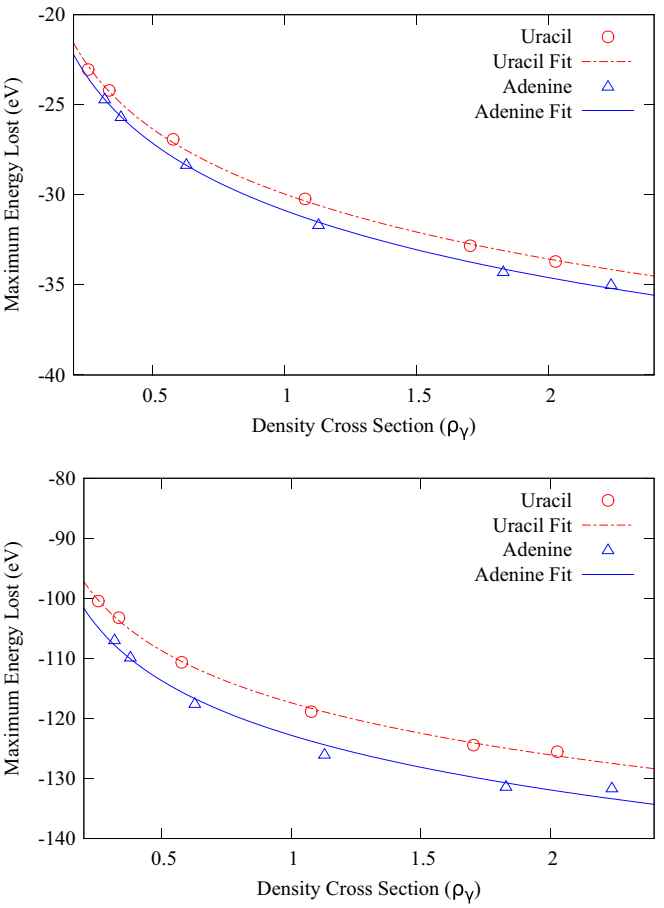


FIG. 8. Maximum energy lost by the projectile as a function of electron density for proton (top) and $\alpha$-particle (bottom) simulations for carbon-carbon bond impact points. A fit to a logarithmic function is shown.

and molecule-particle pair, as shown in Fig. 8; the resulting fit parameters are shown in Table II.

The energy lost by the projectile does not necessarily match the energy absorbed by the molecule because the impact causes some degree of ionization. Either regions of electron density gain enough energy to ionize by directly colliding with the CAP, or the potential of the projectile traps some electron density.

### C. Ionization

The total ionization of the molecular system can be determined by the total electron density in the simulation box after the projectile has exited the simulation box. Any electron density that was transferred to the projectile or ejected to a continuum state will be absorbed by the CAP, leaving only the ionized molecular system. If the system is propagated at times after the projectile has left the simulation box, some additional ionization is observed. However, this continued ionization is an effect of the finite size of the simulation box and is diminished by using a larger box. The ionization as a function of the projectile energy is shown in Fig. 9 for various carbon-carbon bond impact points.

Some trends are clear in the ionization data. At higher projectile speeds, the ionization goes to zero, indicating that the projectile was moving too fast and the electrons were moving too slow to appreciably interact. At intermediate projectile speeds, the interaction causes some ionization, which is higher if it passes through regions of greater electron density, as one would expect. At lower particle energies, the proton and $\alpha$-particle ionization give different results. The $\alpha$-particle simulations seem to converge to an ionization of $\approx 1.9$ regardless of the impact point. For protons the ionization does not converge; however, the ionization from particles of lower speeds would depend upon the alignment of the orbital energy levels, which may not be perfectly represented by the SC potential, and therefore, the lower ionization data are only approximate.

TABLE II. Parameters from the least-squares fit of $y = a \log_{10} x + b$ to the stopping power and electron density data for carbon-carbon bond impact points.

| Molecule | Particle | $a$ | $b$ |
|---|---|---|---|
| Uracil | Proton | $-11.98 \pm 0.19$ | $-29.95 \pm 0.07$ |
| Adenine | Proton | $-12.38 \pm 0.19$ | $-30.87 \pm 0.06$ |
| Uracil | $\alpha$ particle | $-28.9 \pm 0.7$ | $-117.41 \pm 0.24$ |
| Adenine | $\alpha$ particle | $-30.2 \pm 1.7$ | $-122.8 \pm 0.6$ |

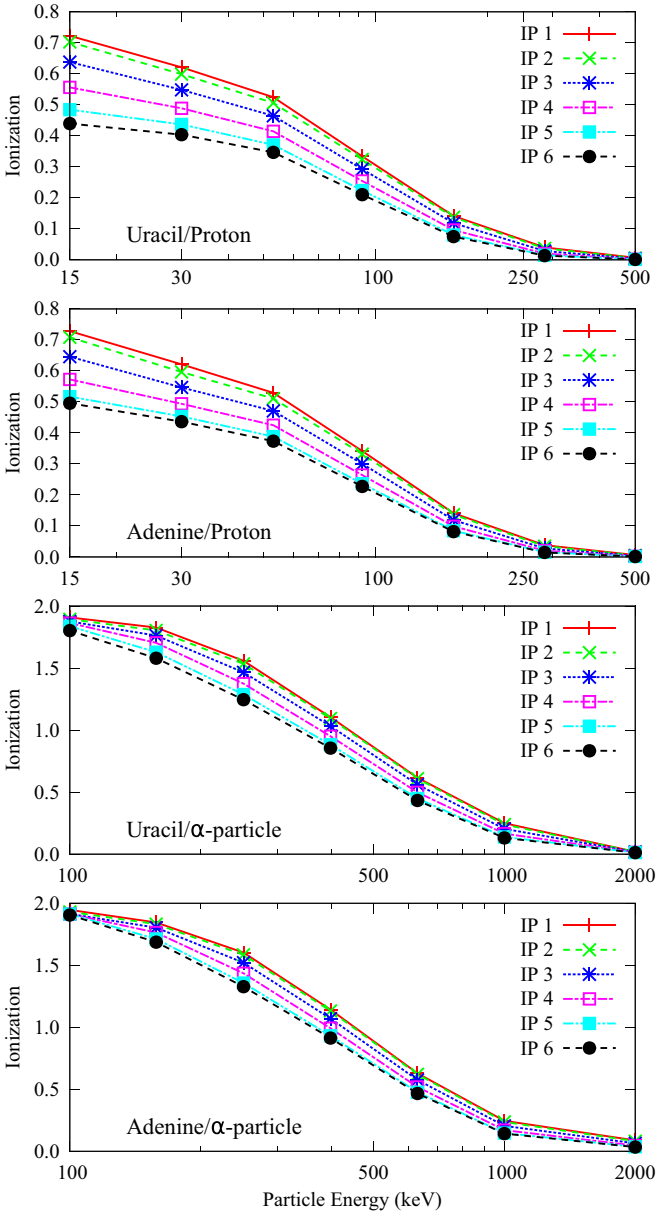


FIG. 9. Ionization of uracil and adenine by protons and $\alpha$ particles for various for carbon-carbon bond impact points as a function of the projectile energy.

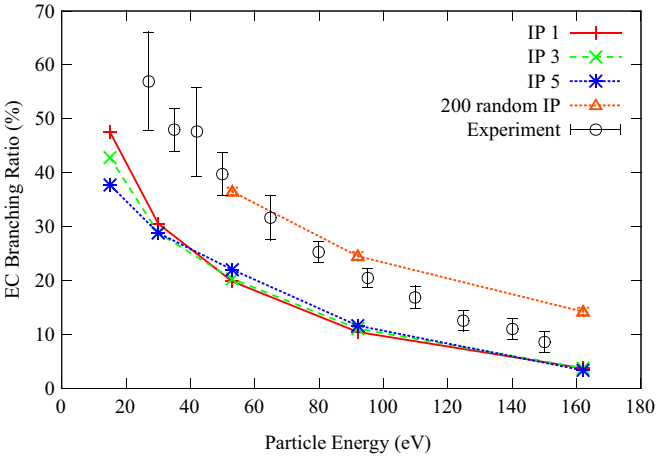


FIG. 10. The calculated EC branching ratio for three carbon-carbon bond impact points for protons incident on uracil and the average of 200 random impact points and incidence angles. Note the error bars for the 200 random impact points are the standard error and represent the error of a finite set of data points. The experimental data were taken from Ref. [8].

The interaction with the projectile can cause the ionized electrons to be localized on the projectile, which is called electron capture (EC), or ejected as free electrons, which is called direct ionization (DI). The ratio of a particular ionization process to the total ionization is called the branching ratio for that process, for which there have been several experimental investigations recently [8,69–71]. It is possible to distinguish between various ionization mechanisms using TDDFT. The branching ratio for the EC ionization process can be determined simply by the probability that an electron would be captured by the projectile and the total ionization probability. For the probability of capture, the electron density localized to the projectile can be used, which is taken to be the probability of finding an electron within 3 Å of the projectile after it has passed sufficiently far from the molecule, where sufficiently far was determined to be 9 Å. The EC branching ratios for three impact points and the average of 200 random impact trajectories are shown for protons incident on uracil in Fig. 10 in comparison to experimental data.

The calculated EC branching ratios for the highly symmetric impact points 1–6 (1, 3, and 5 are shown in Fig. 10) are seen to follow a trend similar to that of the experimental data but are lower by about 10% at lower particle energies. In the experiment, the uracil is in the gas phase, and the incident protons can come from any angle; therefore, the average of a large number of proton trajectories should better reproduce the observed data. The average of 200 random impact points (incident at random angles) lies within the error bars of the experimental data for 53 keV protons and within a few percent for 92 keV protons. At higher energies, the average of the random impact points is higher than the observed experimental trend by about 8%. Considering the limitations of the present TDDFT approach (local-density approximation, pseudopotential representation for core electrons, and a limited number of impact points), the agreement with experiments is promising.

### D. Limitations of the present approach

In previous studies, the issue of the fragmentation of graphene by keV to MeV proton radiation was addressed, with findings indicating that the interaction was insufficient to break chemical bonds [85]. The issue of fragmentation of uracil and adenine is not addressed in this work because of numerous complications. In cases where the projectile passes through the molecule and comes within some critical distance of one of the nuclei, the kinetic energy will be transferred directly to that atom, and fragmentation will occur rapidly and catastrophically. In these cases, the Coulombic interaction from the two nuclei will dominate, and pure Coulombic scattering of the two nuclei can be calculated analytically [98]. In cases

where the projectile passes through the molecule but remains far from any nuclei therein, the molecular fragmentation comes from a combination of ionization and excitation caused by the projectile. The molecular system can be promoted to an excited state, which then decays to the ground state, with the energy transferred to nuclear motion. The ultimate fragmentation event may take several picoseconds to observe [99]. Even neglecting the ionization process, calculation of the fragmentation is quite complicated as initial thermal motion of the atoms can produce numerous fragmentation channels [100], which require hundreds of samples to produce meaningful statistics for fragmenting molecules [99,101]. These factors complicate the calculations on fragmentations caused by ionization in this manner, and calculations concerning molecular fragmentation would require substantially longer run times.

## IV. SUMMARY

Irradiation of uracil and adenine, molecular components of RNA and DNA, by protons and $\alpha$ particles was studied using TDDFT to determine the energy transferred to the molecules, the ionization of the molecules, and their stopping power at keV projectile energies. The energy transfer, ionization, and stopping power were seen to depend upon the impact point and particle energy; however, a logarithmic relationship was found between the maximum of these quantities and the electron density along the path of travel of the particles. The simple relationship between the scattering properties and electron density may allow for easier determination of the penetration depth of ionizing radiation in future studies. As expected, $\alpha$ particles exhibited greater energy transfer than protons by a factor of 3 to 4 in the electron density ranges tested and resulted in significantly more ionization. Additionally, the proton EC ionization branching ratio has been calculated for uracil, showing agreement with experiment for resonant proton impact energies.

The present approach may be extended to simulate the effects of low-energy electrons (as in Ref. [102]) on DNA and RNA since there is evidence that free secondary electrons cause significant single- and double-strand breaks in DNA [4–7,103].

## ACKNOWLEDGMENTS

This work was supported by the National Science Foundation (NSF) under Grants No. Phy 1314463, No. Phy 1560035, and No. IIA1261117. This work used the Extreme Science and Engineering Discovery Environment (XSEDE), which is supported by National Science Foundation Grant No. ACI-1053575.

[1] *Theory of Heavy Ion Collision Physics in Hadron Therapy*, Advances in Quantum Chemistry, edited by D. Belkić, Vol. 65 (Elsevier, Oxford, 2013).
[2] M. E. Galassi, C. Champion, P. F. Weck, R. D. Rivarola, O. Fojn, and J. Hanssen, Phys. Med. Biol. **57**, 2081 (2012).
[3] B. Coupier, B. Farizon, M. Farizon, M. Gaillard, F. Gobet, N. de Castro Faria, G. Jalbert, S. Ouaskit, M. Carré, B. Gstir, G. Hanel, S. Denifl, L. Feketeova, P. Scheier, and T. Märk, Eur. Phys. J. D **20**, 459 (2002).
[4] B. Boudaıffa, P. Cloutier, D. Hunting, M. A. Huels, and L. Sanche, Science **287**, 1658 (2000).
[5] P. Moretto-Capelle and A. Le Padellec, Phys. Rev. A **74**, 062705 (2006).
[6] L. Sanche, Eur. Phys. J. D **35**, 367 (2005).
[7] M. A. Huels, B. Boudaffa, P. Cloutier, D. Hunting, and L. Sanche, J. Am. Chem. Soc. **125**, 4467 (2003).
[8] J. Tabet, S. Eden, S. Feil, H. Abdoul-Carime, B. Farizon, M. Farizon, S. Ouaskit, and T. D. Märk, Phys. Rev. A **81**, 012711 (2010).
[9] P. Mishra and U. Kadhane, Nucl. Instrum. Methods Phys. Res., Sect. B **336**, 12 (2014).
[10] L. Sarkadi, J. Phys. B **49**, 185203 (2016).
[11] C. Champion, M. A. Quinto, J. M. Monti, M. E. Galassi, P. F. Weck, O. A. Fojn, J. Hanssen, and R. D. Rivarola, Phys. Med. Biol. **60**, 7805 (2015).
[12] M. A. H. du Penhoat, P. López-Tarifa, K. K. Ghose, Y. Jeanvoine, M. P. Gaigeot, R. Vuilleumier, M. F. Politis, and M. C. Bacchus-Montabonel, J. Mol. Model. **20**, 2221 (2014).
[13] M.-C. Bacchus-Montabonel, J. Phys. Chem. A **119**, 728 (2015).
[14] M.-C. Bacchus-Montabonel, Eur. Phys. J. D **69**, 107 (2015).
[15] A. Privett and J. Morales, Chem. Phys. Lett. **603**, 82 (2014).
[16] R. Rodriguez-Fernandez, S. A. Vazquez, and E. Martinez-Nunez, Phys. Chem. Chem. Phys. **15**, 7628 (2013).
[17] M. C. Bacchus-Montabonel, M. Łabuda, Y. S. Tergiman, and J. E. Sienkiewicz, Phys. Rev. A **72**, 052706 (2005).
[18] C. Zhou, S. Matsika, M. Kotur, and T. C. Weinacht, J. Phys. Chem. A **116**, 9217 (2012).
[19] P. López-Tarifa, M.-A. H. du Penhoat, R. Vuilleumier, M.-P. Gaigeot, U. Rothlisberger, I. Tavernelli, A. L. Padellec, J.-P. Champeaux, M. Alcamí, P. Moretto-Capelle, F. Martín, and M.-F. Politis, Cent. Eur. J. Phys. **12**, 97 (2014).
[20] P. López-Tarifa, M.-P. Gaigeot, R. Vuilleumier, I. Tavernelli, M. Alcamí, F. Martín, M.-A. Hervé du Penhoat, and M.-F. Politis, Angew. Chem. Int. Ed. **52**, 3160 (2013).
[21] P. López-Tarifa, D. G. Piekarski, E. Rossich, M.-A. H. du Penhoat, R. Vuilleumier, M.-P. Gaigeot, I. Tavernelli, M.-F. Politis, Y. Wang, S. Díaz-Tendero, F. Martín, and M. Alcamí, J. Phys. Conf. Ser. **488**, 012037 (2014).
[22] L. Sadr-Arani, P. Mignon, H. Chermette, and T. Douki, Chem. Phys. Lett. **605**, 108 (2014).
[23] S. Bentzen, Nat. Rev. Cancer **6**, 702 (2006).
[24] F. Stewart, I. Seemann, S. Hoving, and N. Russell, Clin. Oncol. **25**, 617 (2013).
[25] E. Fokas, G. Kraft, H. An, and R. Engenhart-Cabillic, Biochim. Biophys. Acta, Rev. Cancer **1796**, 216 (2009).
[26] G. Kraft, M. Scholz, and U. Bechthold, Radiat. Environ. Biophys. **38**, 229 (1999).
[27] M. A. Tabocchini, A. Campa, and V. Dini, Health Phys. **103**, 547 (2012).
[28] W. P. Levin, H. Kooy, J. S. Loeffler, and T. F. DeLaney, Br. J. Cancer **93**, 849 (2005).
[29] Y. Chen and S. Ahmad, Radiat. Prot. Dosim. **149**, 116 (2012).

[30] M. Biaggi, F. Ballarini, W. Burkard, E. Egger, A. Ferrari, and A. Ottolenghi, Nucl. Instrum. Methods Phys. Res., Sect. B **159**, 89 (1999).

[31] M. Dingfelder, D. Hantke, M. Inokuti, and H. G. Paretzke, Radiat. Phys. Chem. **53**, 1 (1999).

[32] R. H. Ritchie, R. N. Hamm, J. E. Turner, H. A. Wright, and W. E. Bolch, in *Physical and Chemical Mechanisms in Molecular Radiation Biology*, edited by W. A. Glass and M. N. Varma (Springer, Boston, 1991), pp. 99–135.

[33] F. Alvarado, J. Bernard, B. Li, R. Brédy, L. Chen, R. Hoekstra, S. Martin, and T. Schlathölter, Chem. Phys. Chem. **9**, 1254 (2008).

[34] D. T. Ha, Y. Wang, M. Alcamí, E. Itälä, K. Kooser, S. Urpelainen, M. A. Huels, E. Kukk, and F. Martín, J. Phys. Chem. A **118**, 1374 (2014).

[35] E. Itälä, D. T. Ha, K. Kooser, E. Rachlew, M. A. Huels, and E. Kukk, J. Chem. Phys. **133**, 154316 (2010).

[36] S. Maclot, R. Delaunay, D. G. Piekarski, A. Domaracka, B. A. Huber, L. Adoui, F. Martín, M. Alcamí, L. Avaldi, P. Bolognesi, S. Díaz-Tendero, and P. Rousseau, Phys. Rev. Lett. **117**, 073201 (2016).

[37] B. Rudek, A. Arndt, D. Bennett, M. Wang, and H. Rabus, Eur. Phys. J. D **69**, 237 (2015).

[38] J.-C. Poully, J. Miles, S. De Camillis, A. Cassimi, and J. B. Greenwood, Phys. Chem. Chem. Phys. **17**, 7172 (2015).

[39] A. N. Agnihotri, S. Kasthurirangan, S. Nandi, A. Kumar, C. Champion, H. Lekadir, J. Hanssen, P. F. Weck, M. E. Galassi, R. D. Rivarola, O. Fojn, and L. C. Tribedi, J. Phys. B **46**, 185201 (2013).

[40] J. de Vries, R. Hoekstra, R. Morgenstern, and T. Schlathlter, J. Phys. B **35**, 4373 (2002).

[41] H. Luna, W. Wolff, E. C. Montenegro, A. C. Tavares, H. J. Lüdde, G. Schenk, M. Horbatsch, and T. Kirchner, Phys. Rev. A **93**, 052705 (2016).

[42] D. R. Bates and A. Dalgarno, Proc. Phys. Soc., Sec. A **65**, 919 (1952).

[43] D. R. Bates, Proc. R. Soc. London, Ser. A **247**, 294 (1958).

[44] E. Gerjuoy, Rev. Mod. Phys. **33**, 544 (1961).

[45] D. Bates and R. McCarroll, Adv. Phys. **11**, 39 (1962).

[46] I. M. Cheshire, Proc. Phys. Soc. **84**, 89 (1964).

[47] J. E. Golden and J. H. McGuire, Phys. Rev. Lett. **32**, 1218 (1974).

[48] J. E. Golden and J. H. McGuire, Phys. Rev. A **15**, 499 (1977).

[49] D. Belkić, J. Phys. B **11**, 3529 (1978).

[50] D. S. F. Crothers and J. F. McCann, J. Phys. B **16**, 3229 (1983).

[51] T. Kirchner, M. Horbatsch, H. J. Lüdde, and R. M. Dreizler, Phys. Rev. A **62**, 042704 (2000).

[52] T. Kirchner, H. J. Lüdde, M. Horbatsch, and R. M. Dreizler, Phys. Rev. A **61**, 052710 (2000).

[53] M. Horbatsch, Phys. Lett. A **187**, 185 (1994).

[54] T. Kirchner, M. Horbatsch, and H. J. Lüdde, Phys. Rev. A **64**, 012711 (2001).

[55] T. Kirchner and M. Horbatsch, Phys. Rev. A **63**, 062718 (2001).

[56] T. Kirchner, M. Horbatsch, and H. J. Lüdde, Phys. Rev. A **66**, 052719 (2002).

[57] T. Kirchner, A. C. F. Santos, H. Luna, M. M. Sant'Anna, W. S. Melo, G. M. Sigaud, and E. C. Montenegro, Phys. Rev. A **72**, 012707 (2005).

[58] H. J. Lüdde, T. Spranger, M. Horbatsch, and T. Kirchner, Phys. Rev. A **80**, 060702 (2009).

[59] E. C. Montenegro, J. Phys. Conf. Ser. **194**, 012049 (2009).

[60] D. Belkić, J. Math. Chem. **47**, 1366 (2010).

[61] M. Murakami, T. Kirchner, M. Horbatsch, and H. J. Lüdde, Phys. Rev. A **85**, 052704 (2012).

[62] T. Kirchner, M. Murakami, M. Horbatsch, and H. J. Lüdde, in *Theory of Heavy Ion Collision Physics in Hadron Therapy* (Ref. [1]), Chap. 11, pp. 316–335.

[63] H. Nikjoo, P. O'Neill, M. Terrissol, and D. T. Goodhead, Radiat. Environ. Biophys. **38**, 31 (1999).

[64] M. Dingfelder, Health Phys. **103**, 590 (2012).

[65] S. Uehara, L. Toburen, W. Wilson, D. Goodhead, and H. Nikjoo, Radiat. Phys. Chem. **59**, 1 (2000).

[66] A. Itoh, Y. Iriki, M. Imai, C. Champion, and R. D. Rivarola, Phys. Rev. A **88**, 052711 (2013).

[67] F. Gobet, S. Eden, B. Coupier, J. Tabet, B. Farizon, M. Farizon, M. Gaillard, S. Ouaskit, M. Carr, and T. Mrk, Chem. Phys. Lett. **421**, 68 (2006).

[68] L. H. Toburen, M. Y. Nakai, and R. A. Langley, Phys. Rev. **171**, 114 (1968).

[69] F. Gobet, S. Eden, B. Coupier, J. Tabet, B. Farizon, M. Farizon, M. J. Gaillard, M. Carré, S. Ouaskit, T. D. Märk, and P. Scheier, Phys. Rev. A **70**, 062716 (2004).

[70] F. Gobet, B. Farizon, M. Farizon, M. J. Gaillard, M. Carré, M. Lezius, P. Scheier, and T. D. Märk, Phys. Rev. Lett. **86**, 3751 (2001).

[71] J. Tabet, S. Eden, S. Feil, H. Abdoul-Carime, B. Farizon, M. Farizon, S. Ouaskit, and T. Mrk, Int. J. Mass Spectrom. **292**, 53 (2010).

[72] L. Sarkadi, Phys. Rev. A **92**, 062704 (2015).

[73] D. Belkić, R. Gayet, J. Hanssen, and A. Salin, J. Phys. B **19**, 2945 (1986).

[74] C. Champion, M. Galassi, P. Weck, S. Incerti, R. Rivarola, O. Fojn, J. Hanssen, Y. Iriki, and A. Itoh, Nucl. Instrum. Methods Phys. Res., Sect. B **314**, 66 (2013).

[75] E. Runge and E. K. U. Gross, Phys. Rev. Lett. **52**, 997 (1984).

[76] E. P. Silaeva, K. Uchida, Y. Suzuki, and K. Watanabe, Phys. Rev. B **92**, 155401 (2015).

[77] A. C.-Uranga, U. De Giovannini, E. Räsänen, M. J. T. Oliveira, D. J. Mowbray, G. M. Nikolopoulos, E. T. Karamatskos, D. Markellos, P. Lambropoulos, S. Kurth, and A. Rubio, Phys. Rev. A **90**, 033412 (2014).

[78] A. Russakoff, S. Bubin, X. Xie, S. Erattupuzha, M. Kitzler, and K. Varga, Phys. Rev. A **91**, 023422 (2015).

[79] B. F. E. Curchod, U. Rothlisberger, and I. Tavernelli, Chem. Phys. Chem. **14**, 1314 (2013).

[80] A. Russakoff and K. Varga, Phys. Rev. A **92**, 053413 (2015).

[81] X. Xie, S. Roither, M. Schöffler, H. Xu, S. Bubin, E. Lötstedt, S. Erattuphuza, A. Iwasaki, D. Kartashov, K. Varga, G. G. Paulus, A. Baltuška, K. Yamanouchi, and M. Kitzler, Phys. Rev. A **89**, 023429 (2014).

[82] Y. Li, S. He, A. Russakoff, and K. Varga, Phys. Rev. E **94**, 023314 (2016).

[83] A. Russakoff, Y. Li, S. He, and K. Varga, J. Chem. Phys. **144**, 204125 (2016).

[84] C. Covington, D. Kidd, J. Gilmer, and K. Varga, Phys. Rev. A **95**, 013414 (2017).

[85] S. Bubin, B. Wang, S. Pantelides, and K. Varga, Phys. Rev. B **85**, 235435 (2012).

[86] J. Wang, C.-Z. Gao, F. Calvayrac, and F.-S. Zhang, J. Chem. Phys. **140**, 124306 (2014).

[87] J. P. Perdew and A. Zunger, Phys. Rev. B **23**, 5048 (1981).
[88] N. Troullier and J. L. Martins, Phys. Rev. B **43**, 1993 (1991).
[89] P. Ehrenfest, Z. Phys. **45**, 455 (1927).
[90] D. E. Manolopoulos, J. Chem. Phys. **117**, 9552 (2002).
[91] Q. Su and J. H. Eberly, Phys. Rev. A **44**, 5997 (1991).
[92] C. K. Law, Q. Su, and J. H. Eberly, Phys. Rev. A **44**, 7844 (1991).
[93] Z. Zhou, D. Zhang, Z. Zhao, and J. Yuan, Phys. Rev. A **79**, 063413 (2009).
[94] R. Taïeb, V. Véniard, J. Wassaf, and A. Maquet, Phys. Rev. A **68**, 033403 (2003).
[95] M. Valiev, E. Bylaska, N. Govind, K. Kowalski, T. Straatsma, H. v. Dam, D. Wang, J. Nieplocha, E. Apra, T. Windus, and W. de Jong, Comput. Phys. Commun. **181**, 1477 (2010).
[96] H. Akima, J. ACM **22**, 357 (1996).
[97] A. C. Miller, Bicubic interpolation FORTRAN90 code, http://jblevins.org/mirror/amiller/toms760.f90.
[98] R. Bass, *Nuclear Reactions with Heavy Ions* (Springer, Berlin, 1980).
[99] S. Grimme, Angew. Chem., Int. Ed. **52**, 6306 (2013).
[100] E. R. Molina, J.-Y. Salpin, R. Spezia, and E. Martinez-Nunez, Phys. Chem. Chem. Phys. **18**, 14980 (2016).
[101] C. A. Bauer and S. Grimme, Org. Biomol. Chem. **12**, 8737 (2014).
[102] C. Champion, D. Oubaziz, H. Aouchiche, Y. V. Popov, and C. Dal Cappello, Phys. Rev. A **81**, 032704 (2010).
[103] E. Alizadeh and L. Sanche, Chem. Rev. **112**, 5578 (2012).